The Astrophysical Journal Supplement Series, 196:24 (9pp), 2011 October doi:10.1088/0067-0049/196/2/24

ELECTRON-IMPACT EXCITATION OF Cr II: A THEORETICAL CALCULATION OF EFFECTIVE COLLISION STRENGTHS FOR OPTICALLY ALLOWED TRANSITIONS

I. R. Wasson, C. A. Ramsbottom, and M. P. Scott
Department of Applied Mathematics and Theoretical Physics, Queen's University, Belfast, UK; iwasson01@qub.ac.uk
Received 2011 May 19; accepted 2011 September 1; published 2011 September 30

ABSTRACT

In this paper, we present electron-impact excitation collision strengths and Maxwellian averaged effective collision strengths for the complicated iron-peak ion Cr II. We consider specifically the allowed lines for transitions from the $3d^5$ and $3d^4 4s$ even parity configuration states to the $3d^4 4p$ odd parity configuration levels. The parallel suite of *R*-Matrix packages, RMATRX II, which have recently been extended to allow for the inclusion of relativistic effects, were used to compute the collision cross sections. A total of 108 LSπ /280 $J\pi$ levels from the basis configurations $3d^5$, $3d^4 4s$, and $3d^4 4p$ were included in the wavefunction representation of the target including all doublet, quartet, and sextet terms. Configuration interaction and correlation effects were carefully considered by the inclusion of seven more configurations and a pseudo-corrector $\overline{4d}$ type orbital. The 10 configurations incorporated into the Cr II model thus listed are $3d^5$, $3d^4 4s$, $3d^4 4p$, $3d^3 4s^2$, $3d^3 4p^2$, $3d^3 4s 4p$, $3d^4\overline{4d}$, $3d^3 4s\overline{4d}$, $3d^3 4p\overline{4d}$, and $3d^3\overline{4d}^2$, constituting the largest Cr II target model considered to date in a scattering calculation. The Maxwellian averaged effective collision strengths are computed for a wide range of electron temperatures 2000–100,000 K which are astrophysically significant. Care has been taken to ensure that the partial wave contributions to the collision strengths for these allowed lines have converged with "top-up" from the Burgess–Tully sum rule incorporated. Comparisons are made with the results of Bautista et al. and significant differences are found for some of the optically allowed lines considered.

Key words: atomic data – atomic processes – methods: numerical – plasmas – scattering

Online-only material: color figures, machine-readable tables

1. INTRODUCTION

Cr II is a member of the astrophysically significant, yet notoriously difficult to model, iron-peak elements. These open *d*-shell ions, which range from scandium ($Z = 21$) to copper ($Z = 29$) in the periodic table, occur in abundance in many different astrophysical bodies and indeed, emission and absorption lines of these elements have been identified in the spectra of a wide variety of astronomical objects at all wavelengths from the infrared to the ultraviolet. Modeling these ions, however, is a difficult task due to their complicated structures caused by the presence of the open *d*-shells. Hundreds of fine-structure states need to be included to properly represent the Cr II ion leading to thousands of coupled channels in the scattering calculation.

Atomic data for Cr II are well known to be of critical importance in the analysis of a broad range of stellar and nebular spectra. For example, Iijima & Nakanishi (2008) reported the observation of prominent emission lines of Cr II, as well as many other iron-peak elements, during the early decline stage of the peculiar, explosive object Nova (V445) Puppis 2000. In addition, Luftinger et al. (2010) used Doppler and Magnetic Doppler imaging techniques to derive the magnetic field geometry of the *CoRoT* CP2 target star HD 50773. Surface abundance distributions were derived for Mg, Si, Ca, Ti, Cr, Fe, Ni, Y, and Cu, with seven lines of Cr II used for abundance analysis in the co-added spectrum of HD 50773. Finally, Bergemann & Cescutti (2010) have recently applied theoretical atomic data consisting of 114 levels for Cr I and 225 levels for Cr II when investigating non-local thermodynamic equilibrium abundances of Cr in metal-poor stars. This work was of particular interest in looking at star formation theory and the early evolution stages of a star.

Up until very recently there was a distinct paucity of atomic data available in the literature for the electron-impact excitation of Cr II. The earliest sophisticated calculation performed for this ion was reported by Bautista et al. (2009) where electron-impact collision strengths for transitions among the lowest 162 fine-structure levels of Cr II were evaluated but not published. Wasson et al. (2010) subsequently extended this calculation and computed the fine-structure collisional data for all forbidden transitions among the lowest 280 levels of Cr II arising from the basic configurations $3d^5$, $3d^4 4s$, and $3d^4 4p$. This latter calculation corresponded to a substantial 1932 coupled channel problem. The authors, however, concentrated on the fine-structure lines among the lowest 74 fine-structure levels corresponding to the $3d^5$ and $3d^4 4s$ even parity configuration states. These transitions converge much more quickly than the allowed lines and the collision strength contributions from each of the $J\pi$ partial waves were found to have well converged before a total angular momentum value of $2J = 14$ had been reached. The same is not true for the allowed transitions considered in the present publications and the contributions from the higher partial waves need to be taken into account. In this paper we therefore concentrate on the optically allowed transitions from the $3d^5$ and $3d^4 4s$ even parity levels to the $3d^4 4p$ odd parity states. The collision strengths are evaluated for a very fine mesh of incident electron energies and the contributions to the collision strengths from the higher partial waves have fully converged.

2. THE TARGET MODEL

The theoretical Cr II model adopted in the present calculation has been described in detail by Wasson et al. (2010) and will only be summarized here. A total of 108 LS/280*jj* levels formed from the basis configurations $3d^5$, $3d^4 4s$, and $3d^4 4p$

Table 1
Energy Levels for All Fine-structure Target States of Cr II Considered in the Present Work

Index	Config.	LS	J	Energy	Index	Config.	LS	J	Energy
1	$3d^5$	$^6S^e$	5/2	0.0000000	65	$3d^4(a\ 1G)4s$	$^2G^e$	9/2	0.3629062
2	$3d^4(5D)4s$	$^6D^e$	1/2	0.1090039	66	$3d^5$	$^2F^e$	7/2	0.3633863
3	$3d^4(5D)4s$	$^6D^e$	3/2	0.1096489	67	$3d^4(1I)4s$	$^2I^e$	13/2	0.3663484
4	$3d^4(5D)4s$	$^6D^e$	5/2	0.1106990	68	$3d^4(1I)4s$	$^2I^e$	11/2	0.3665872
5	$3d^4(5D)4s$	$^6D^e$	7/2	0.1121209	69	$3d^4(1S)4s$	$^2S^e$	1/2	0.3682891
6	$3d^4(5D)4s$	$^6D^e$	9/2	0.1138759	70	$3d^4(3D)4s$	$^2D^e$	5/2	0.3909149
7	$3d^4(5D)4s$	$^4D^e$	1/2	0.1779544	71	$3d^4(3D)4s$	$^2D^e$	3/2	0.3917226
8	$3d^4(5D)4s$	$^4D^e$	3/2	0.1788922	72	$3d^5$	$^2S^e$	1/2	0.4037556
9	$3d^4(5D)4s$	$^4D^e$	5/2	0.1804114	73	$3d^4(1D)4s$	$^2D^e$	3/2	0.4161696
10	$3d^4(5D)4s$	$^4D^e$	7/2	0.1824721	74	$3d^4(1D)4s$	$^2D^e$	5/2	0.4167274
11	$3d^5$	$^4G^e$	5/2	0.1869195	75	$3d^4(5D)4p$	$^6F^o$	1/2	0.4266858
12	$3d^5$	$^4G^e$	11/2	0.1869199	76	$3d^4(5D)4p$	$^6F^o$	3/2	0.4274310
13	$3d^5$	$^4G^e$	7/2	0.1869721	77	$3d^4(5D)4p$	$^6F^o$	5/2	0.4286629
14	$3d^5$	$^4G^e$	9/2	0.1869857	78	$3d^4(5D)4p$	$^6F^o$	7/2	0.4303659
15	$3d^5$	$^4P^e$	5/2	0.1988613	79	$3d^5$	$^2D^e$	5/2	0.4315251
16	$3d^5$	$^4P^e$	1/2	0.1988733	80	$3d^5$	$^2D^e$	3/2	0.4316899
17	$3d^5$	$^4P^e$	3/2	0.1988758	81	$3d^4(5D)4p$	$^6F^o$	9/2	0.4325285
18	$3d^5$	$^4D^e$	7/2	0.2281237	82	$3d^4(5D)4p$	$^6F^o$	11/2	0.4351444
19	$3d^5$	$^4D^e$	1/2	0.2281392	83	$3d^4(5D)4p$	$^6P^o$	3/2	0.4410433
20	$3d^5$	$^4D^e$	3/2	0.2282067	84	$3d^4(5D)4p$	$^6P^o$	5/2	0.4418831
21	$3d^5$	$^4D^e$	5/2	0.2282427	85	$3d^4(5D)4p$	$^6P^o$	7/2	0.4431681
22	$3d^4(3P)4s$	$^4P^e$	1/2	0.2729414	86	$3d^4(5D)4p$	$^4P^o$	1/2	0.4442365
23	$3d^5$	$^2I^e$	11/2	0.2746857	87	$3d^4(5D)4p$	$^4P^o$	3/2	0.4465745
24	$3d^5$	$^2I^e$	13/2	0.2747453	88	$3d^4(5D)4p$	$^6D^o$	5/2	0.4497263
25	$3d^4(3H)4s$	$^4H^e$	7/2	0.2748087	89	$3d^4(5D)4p$	$^6D^o$	1/2	0.4510110
26	$3d^4(3H)4s$	$^4H^e$	9/2	0.2753738	90	$3d^4(5D)4p$	$^6D^o$	3/2	0.4516655
27	$3d^4(3H)4s$	$^4H^e$	11/2	0.2761001	91	$3d^4(5D)4p$	$^6D^o$	7/2	0.4524052
28	$3d^4(3P)4s$	$^4P^e$	3/2	0.2761815	92	$3d^4(5D)4p$	$^4P^o$	5/2	0.4529571
29	$3d^4(3H)4s$	$^4H^e$	13/2	0.2769505	93	$3d^4(5D)4p$	$^6D^o$	9/2	0.4541604
30	$3d^4(3P)4s$	$^4P^e$	5/2	0.2812574	94	$3d^4(1F)4s$	$^2F^e$	7/2	0.4617135
31	$3d^4(3F)4s$	$^4F^e$	3/2	0.2832484	95	$3d^4(1F)4s$	$^2F^e$	5/2	0.4618992
32	$3d^4(3F)4s$	$^4F^e$	5/2	0.2835623	96	$3d^4(5D)4p$	$^4F^o$	3/2	0.4700690
33	$3d^4(3F)4s$	$^4F^e$	7/2	0.2840288	97	$3d^4(5D)4p$	$^4F^o$	5/2	0.4708466
34	$3d^4(3F)4s$	$^4F^e$	9/2	0.2844914	98	$3d^4(5D)4p$	$^4F^o$	7/2	0.4719346
35	$3d^5$	$^2D^e$	5/2	0.2856902	99	$3d^4(5D)4p$	$^4F^o$	9/2	0.4733363
36	$3d^5$	$^2D^e$	3/2	0.2873336	100	$3d^5$	$^2G^e$	7/2	0.4765723
37	$3d^5$	$^2F^e$	7/2	0.2948464	101	$3d^5$	$^2G^e$	9/2	0.4767838
38	$3d^5$	$^2F^e$	5/2	0.2971038	102	$3d^4(5D)4p$	$^4D^o$	1/2	0.4958931
39	$3d^5$	$^4F^e$	7/2	0.2992296	103	$3d^4(5D)4p$	$^4D^o$	3/2	0.4966358
40	$3d^5$	$^4F^e$	3/2	0.2993032	104	$3d^4(5D)4p$	$^4D^o$	5/2	0.4977849
41	$3d^5$	$^4F^e$	9/2	0.2993903	105	$3d^4(5D)4p$	$^4D^o$	7/2	0.4992325
42	$3d^5$	$^4F^e$	5/2	0.2993961	106	$3d^4(3F)4s$	$^4F^e$	9/2	0.4999901
43	$3d^4(3G)4s$	$^4G^e$	5/2	0.3045269	107	$3d^4(3F)4s$	$^4F^e$	3/2	0.4999993
44	$3d^4(3G)4s$	$^4G^e$	7/2	0.3054666	108	$3d^4(3F)4s$	$^4F^e$	5/2	0.5001352
45	$3d^4(3G)4s$	$^4G^e$	9/2	0.3063581	109	$3d^4(3F)4s$	$^4F^e$	7/2	0.5001756
46	$3d^4(3G)4s$	$^4G^e$	11/2	0.3070435	110	$3d^4(3P)4s$	$^4P^e$	5/2	0.5014070
47	$3d^4(3H)4s$	$^2H^e$	9/2	0.3155802	111	$3d^4(3P)4s$	$^4P^e$	3/2	0.5048301
48	$3d^4(3P)4s$	$^2P^e$	1/2	0.3158387	112	$3d^4(3P)4s$	$^4P^e$	1/2	0.5069029
49	$3d^4(3H)4s$	$^2H^e$	11/2	0.3172387	113	$3d^4(3P)4s$	$^2P^e$	3/2	0.5388351
50	$3d^4(3P)4s$	$^2P^e$	3/2	0.3221863	114	$3d^4(3P)4s$	$^2P^e$	1/2	0.5424471
51	$3d^4(3F)4s$	$^2F^e$	5/2	0.3241302	115	$3d^4(3F)4s$	$^2F^e$	7/2	0.5428423
52	$3d^4(3F)4s$	$^2F^e$	7/2	0.3244792	116	$3d^4(3F)4s$	$^2F^e$	5/2	0.5429112
53	$3d^5$	$^2H^e$	9/2	0.3245051	117	$3d^4(3G)4s$	$^2G^e$	9/2	0.5712633
54	$3d^5$	$^2H^e$	11/2	0.3253903	118	$3d^4(3G)4s$	$^2G^e$	7/2	0.5713792
55	$3d^5$	$^2G^e$	7/2	0.3289816	119	$3d^4(3H)4p$	$^4H^o$	7/2	0.5795737
56	$3d^5$	$^2G^e$	9/2	0.3305395	120	$3d^4(3H)4p$	$^4H^o$	9/2	0.5805341
57	$3d^4(3D)4s$	$^4D^e$	7/2	0.3487379	121	$3d^4(a\ 3P)4p$	$^4D^o$	1/2	0.5814051
58	$3d^4(3D)4s$	$^4D^e$	5/2	0.3491504	122	$3d^4(3H)4p$	$^4H^o$	11/2	0.5818321
59	$3d^4(3D)4s$	$^4D^e$	3/2	0.3495839	123	$3d^4(3H)4p$	$^4H^o$	13/2	0.5834887
60	$3d^4(3D)4s$	$^4D^e$	1/2	0.3498919	124	$3d^4(a\ 3P)4p$	$^4D^o$	3/2	0.5837730
61	$3d^4(3G)4s$	$^2G^e$	7/2	0.3509189	125	$3d^4(a\ 3P)4p$	$^4D^o$	5/2	0.5873003
62	$3d^4(3G)4s$	$^2G^e$	9/2	0.3514117	126	$3d^5\ *$	$^2P^e$	3/2	0.5914730
63	$3d^4(a\ 1G)4s$	$^2G^e$	7/2	0.3616247	127	$3d^4(a\ 3P)4p$	$^4D^o$	7/2	0.5916353
64	$3d^5$	$^2F^e$	5/2	0.3621563	128	$3d^5\ *$	$^2P^e$	1/2	0.5924667

Table 1
(Continued)

Index	Config.	LS	J	Energy	Index	Config.	LS	J	Energy
129	$3d^4(a\ 3P)4p$	$^2S^o$	1/2	0.5925913	193	$3d^4(3D)4p$	$^4D^o$	7/2	0.6696501
130	$3d^4(a\ 3F)4p$	$^4G^o$	5/2	0.5937498	194	$3d^4(a\ 1G)4p$	$^2F^o$	7/2	0.6753795
131	$3d^4(3H)4p$	$^4I^o$	9/2	0.5943056	195	$3d^4(3D)4p$	$^4F^o$	3/2	0.6768277
132	$3d^4(a\ 3F)4p$	$^4G^o$	7/2	0.5946640	196	$3d^4(3D)4p$	$^4F^o$	5/2	0.6772425
133	$3d^4(a\ 3F)4p$	$^4G^o$	9/2	0.5958219	197	$3d^4(1I)4p$	$^2I^o$	11/2	0.6781808
134	$3d^4(3H)4p$	$^4I^o$	11/2	0.5961464	198	$3d^4(3D)4p$	$^4F^o$	7/2	0.6781979
135	$3d^4(3H)4p$	$^2G^o$	7/2	0.5972707	199	$3d^4(1I)4p$	$^2K^o$	13/2	0.6782026
136	$3d^4(3H)4p$	$^4I^o$	13/2	0.5979547	200	$3d^4(a\ 1G)4p$	$^2F^o$	5/2	0.6783116
137	$3d^4(3H)4p$	$^2G^o$	9/2	0.5985205	201	$3d^4(a\ 1G)4p$	$^2H^o$	9/2	0.6784908
138	$3d^4(a\ 3F)4p$	$^4G^o$	11/2	0.5987886	202	$3d^4(3D)4p$	$^4P^o$	5/2	0.6787473
139	$3d^4(3H)4p$	$^4I^o$	15/2	0.5997277	203	$3d^4(3D)4p$	$^4F^o$	9/2	0.6789314
140	$3d^4(a\ 3P)4p$	$^4P^o$	1/2	0.6037729	204	$3d^4(a\ 1G)4p$	$^2H^o$	11/2	0.6807841
141	$3d^4(a\ 3P)4p$	$^4P^o$	3/2	0.6046692	205	$3d^4(3D)4p$	$^4P^o$	3/2	0.6808763
142	$3d^4(a\ 3P)4p$	$^2P^o$	3/2	0.6073534	206	$3d^4(1I)4p$	$^2I^o$	13/2	0.6811104
143	$3d^4(a\ 3P)4p$	$^4P^o$	5/2	0.6080590	207	$3d^4(3D)4p$	$^2P^o$	1/2	0.6821179
144	$3d^4(a\ 3P)4p$	$^2P^o$	1/2	0.6093814	208	$3d^4(3D)4p$	$^4P^o$	1/2	0.6827248
145	$3d^4(a\ 3F)4p$	$^4F^o$	5/2	0.6106587	209	$3d^4(1I)4p$	$^2K^o$	15/2	0.6830743
146	$3d^4(a\ 3F)4p$	$^4F^o$	3/2	0.6111904	210	$3d^4(3D)4p$	$^2P^o$	3/2	0.6833111
147	$3d^4(3H)4p$	$^4G^o$	7/2	0.6135905	211	$3d^4(a\ 1G)4p$	$^2G^o$	7/2	0.6899794
148	$3d^4(3H)4p$	$^4G^o$	5/2	0.6136835	212	$3d^4(a\ 1G)4p$	$^2G^o$	9/2	0.6908314
149	$3d^4(3H)4p$	$^4G^o$	9/2	0.6137679	213	$3d^4(3D)4p$	$^2F^o$	7/2	0.7005727
150	$3d^4(3H)4p$	$^4G^o$	11/2	0.6139123	214	$3d^4(3D)4p$	$^2F^o$	5/2	0.7015630
151	$3d^4(a\ 3F)4p$	$^2D^o$	3/2	0.6140064	215	$3d^4(1I)4p$	$^2H^o$	11/2	0.7023943
152	$3d^4(a\ 3F)4p$	$^2D^o$	5/2	0.6140765	216	$3d^4(1I)4p$	$^2H^o$	9/2	0.7041378
153	$3d^4(a\ 3F)4p$	$^4F^o$	7/2	0.6141344	217	$3d^4(a\ 1S)4p$	$^2P^o$	3/2	0.7081750
154	$3d^4(a\ 3F)4p$	$^4F^o$	9/2	0.6146361	218	$3d^4(a\ 1S)4p$	$^2P^o$	1/2	0.7087586
155	$3d^4(3H)4p$	$^2I^o$	11/2	0.6151606	219	$3d^4(3D)4p$	$^2D^o$	5/2	0.7101977
156	$3d^4(3H)4p$	$^2I^o$	13/2	0.6159149	220	$3d^4(3D)4p$	$^2D^o$	3/2	0.7117861
157	$3d^4(a\ 3F)4p$	$^4D^o$	1/2	0.6183818	221	$3d^4(a\ 1D)4p$	$^2D^o$	3/2	0.7316380
158	$3d^4(a\ 3F)4p$	$^4D^o$	5/2	0.6184566	222	$3d^4(a\ 1D)4p$	$^2D^o$	5/2	0.7328422
159	$3d^4(a\ 3F)4p$	$^4D^o$	3/2	0.6184787	223	$3d^4(a\ 1D)4p$	$^2F^o$	5/2	0.7402483
160	$3d^4(a\ 3F)4p$	$^4D^o$	7/2	0.6185259	224	$3d^4(a\ 1D)4p$	$^2F^o$	7/2	0.7420651
161	$3d^4(a\ 3P)4p$	$^4S^o$	3/2	0.6224463	225	$3d^4(a\ 1D)4p$	$^2P^o$	1/2	0.7550193
162	$3d^4(3H)4p$	$^2H^o$	9/2	0.6240071	226	$3d^4(a\ 1D)4p$	$^2P^o$	3/2	0.7556211
163	$3d^4(a\ 3F)4p$	$^2F^o$	5/2	0.6249769	227	$3d^4(1F)4p$	$^2F^o$	5/2	0.7709754
164	$3d^4(3H)4p$	$^2H^o$	11/2	0.6263846	228	$3d^4(1F)4p$	$^2F^o$	7/2	0.7716342
165	$3d^4(a\ 3F)4p$	$^2F^o$	7/2	0.6265857	229	$3d^4(1F)4p$	$^2G^o$	7/2	0.7797995
166	$3d^4(3G)4p$	$^4H^o$	7/2	0.6273458	230	$3d^4(1F)4p$	$^2G^o$	9/2	0.7831328
167	$3d^4(3G)4p$	$^4H^o$	9/2	0.6287045	231	$3d^4(1F)4p$	$^2D^o$	5/2	0.7883120
168	$3d^4(3G)4p$	$^4H^o$	11/2	0.6303265	232	$3d^44s\ *$	$^2D^e$	3/2	0.7889768
169	$3d^4(a\ 3P)4p$	$^2D^o$	3/2	0.6319466	233	$3d^44s\ *$	$^2D^e$	5/2	0.7889804
170	$3d^4(3G)4p$	$^4H^o$	13/2	0.6323118	234	$3d^4(1F)4p$	$^2D^o$	3/2	0.7920637
171	$3d^4(3G)4p$	$^4F^o$	5/2	0.6331292	235	$3d^4(b\ 3P)4p$	$^4P^o$	3/2	0.8148759
172	$3d^4(3G)4p$	$^4F^o$	9/2	0.6333144	236	$3d^4(b\ 3P)4p$	$^4P^o$	5/2	0.8151570
173	$3d^4(3G)4p$	$^4F^o$	7/2	0.6333855	237	$3d^4(b\ 3P)4p$	$^4P^o$	1/2	0.8156557
174	$3d^4(3G)4p$	$^4F^o$	3/2	0.6345934	238	$3d^4(b\ 3P)4p$	$^4D^o$	7/2	0.8221307
175	$3d^4(a\ 3F)4p$	$^2G^o$	7/2	0.6370075	239	$3d^4(b\ 3P)4p$	$^4D^o$	5/2	0.8224926
176	$3d^4(a\ 3P)4p$	$^2D^o$	5/2	0.6374681	240	$3d^4(b\ 3F)4p$	$^4F^o$	3/2	0.8225284
177	$3d^4(a\ 3F)4p$	$^2G^o$	9/2	0.6388676	241	$3d^4(b\ 3F)4p$	$^4F^o$	5/2	0.8241655
178	$3d^4(3G)4p$	$^4G^o$	5/2	0.6407742	242	$3d^4(b\ 3P)4p$	$^4D^o$	3/2	0.8242461
179	$3d^4(3G)4p$	$^2H^o$	9/2	0.6414787	243	$3d^4(b\ 3P)4p$	$^4D^o$	1/2	0.8244726
180	$3d^4(3G)4p$	$^2H^o$	11/2	0.6415212	244	$3d^4(b\ 3F)4p$	$^4F^o$	7/2	0.8246036
181	$3d^4(3G)4p$	$^4G^o$	7/2	0.6417780	245	$3d^4(b\ 3F)4p$	$^4F^o$	9/2	0.8255033
182	$3d^4(3G)4p$	$^2F^o$	5/2	0.6432125	246	$3d^4(b\ 3F)4p$	$^2F^o$	5/2	0.8265807
183	$3d^4(3G)4p$	$^4G^o$	9/2	0.6440753	247	$3d^4(b\ 3F)4p$	$^2F^o$	7/2	0.8277104
184	$3d^4(3G)4p$	$^2F^o$	7/2	0.6456525	248	$3d^4(b\ 3F)4p$	$^4G^o$	5/2	0.8299697
185	$3d^4(3G)4p$	$^4G^o$	11/2	0.6459038	249	$3d^4(b\ 3F)4p$	$^4G^o$	7/2	0.8303716
186	$3d^5\ *$	$^2D^e$	5/2	0.6527753	250	$3d^4(b\ 3F)4p$	$^4G^o$	9/2	0.8309793
187	$3d^5\ *$	$^2D^e$	3/2	0.6529060	251	$3d^4(b\ 3F)4p$	$^4G^o$	11/2	0.8319147
188	$3d^4(3G)4p$	$^2G^o$	7/2	0.6620215	252	$3d^4(b\ 3P)4p$	$^2D^o$	5/2	0.8331349
189	$3d^4(3G)4p$	$^2G^o$	9/2	0.6626430	253	$3d^4(b\ 3P)4p$	$^2D^o$	3/2	0.8343227
190	$3d^4(3D)4p$	$^4D^o$	1/2	0.6689333	254	$3d^4(b\ 3P)4p$	$^4S^o$	3/2	0.8439445
191	$3d^4(3D)4p$	$^4D^o$	3/2	0.6689785	255	$3d^4(b\ 3F)4p$	$^4D^o$	7/2	0.8523228
192	$3d^4(3D)4p$	$^4D^o$	5/2	0.6691991	256	$3d^4(b\ 3F)4p$	$^2G^o$	9/2	0.8533235

Table 1
(Continued)

Index	Config.	LS	J	Energy	Index	Config.	LS	J	Energy
257	$3d^4(b\ 3F)4p$	$^4D^o$	5/2	0.8535923	269	$3d^4(b\ 3F)4p$	$^2D^o$	3/2	0.8959114
258	$3d^4(b\ 3F)4p$	$^4D^o$	3/2	0.8544954	270	$3d^4(b\ 1G)4p$	$^2F^o$	7/2	0.9027851
259	$3d^4(b\ 3F)4p$	$^4D^o$	1/2	0.8547714	271	$3d^4(b\ 1G)4p$	$^2F^o$	5/2	0.9043771
260	$3d^4(b\ 3F)4p$	$^2G^o$	7/2	0.8547811	272	$3d^44s*$	$^2P^e$	1/2	0.9805123
261	$3d^4(b\ 3P)4p$	$^2P^o$	3/2	0.8600823	273	$3d^44p*$	$^2P^o$	3/2	1.0399800
262	$3d^4(b\ 3P)4p$	$^2P^o$	1/2	0.8622832	274	$3d^44p*$	$^2P^o$	1/2	1.0422870
263	$3d^4(b\ 3P)4p$	$^2S^o$	1/2	0.8770512	275	$3d^44p*$	$^2D^o$	3/2	1.0515680
264	$3d^4(b\ 1G)4p$	$^2H^o$	9/2	0.8883032	276	$3d^44p*$	$^2F^o$	5/2	1.0560210
265	$3d^4(b\ 1G)4p$	$^2G^o$	7/2	0.8905647	277	$3d^44p*$	$^2F^o$	5/2	1.0667810
266	$3d^4(b\ 1G)4p$	$^2H^o$	11/2	0.8921244	278	$3d^44p*$	$^2G^o$	7/2	1.0701220
267	$3d^4(b\ 1G)4p$	$^2G^o$	9/2	0.8921702	279	$3d^44p*$	$^2S^o$	1/2	1.1736580
268	$3d^4(b\ 3F)4p$	$^2D^o$	5/2	0.8949306	280	$3d^44p*$	$^2D^o$	3/2	1.1736820

Note. * represents unobserved levels.

were included in the wavefunction representation of the Cr II ion. These states were represented by configuration-interaction wavefunction expansions in terms of nine orthogonal basis orbitals, eight spectroscopic ($1s$, $2s$, $2p$, $3s$, $3p$, $3d$, $4s$, and $4p$) and one pseudo-type corrector orbital ($\overline{4d}$) included to account for additional correlation effects. The parameters utilized for the Hartree–Fock orbitals were taken from the tables of Clementi & Roetti (1974) while those for the remaining non-Hartree–Fock orbitals were obtained variationally using the CIV3 code of Hibbert (1975). All parameter values which describe the orbital basis can be found in the tabulations of Wasson et al. (2010) and will not be reproduced here. In Table 1, we present the target state energies in Rydbergs relative to the $3d^5\ ^6S^e_{5/2}$ ground state for all 280 fine-structure levels considered. These energies have been shifted to their observed experimental values listed in the NIST compilation where available, to ensure that thresholds lie in their exact positions. In Table 1, each target level is assigned an index value ranging from 1 to 280 which will be used again in subsequent tables when denoting a particular transition.

The RMATRX II R-matrix suite of codes (Burke et al. 1994) were used in the present calculation to compute the diagonalized Hamiltonian matrices in the internal region using LS coupling. Relativistic effects were incorporated by transforming the R-matrix in LS coupling at energy E into an R-matrix in pair coupling (private communication with V. M. Burke in association with Sunderland et al. 2002). In this method the energy independent surface amplitudes are transformed at the R-matrix boundary and the term splitting in the target is taken into account by employing the term coupling coefficients. One of the advantages of using this method, over other transformation procedures, is that it allows us to include fine-structure channels in the external region as the transformation occurs on the R-matrix boundary as opposed to the asymptotic boundary. Finally, the PSTGF external region code of Ballance & Griffin (2004) was used to compute the collision strengths over a very fine mesh of incident electron energies to ensure proper delineation of the complex resonance structures which dominate the low-energy collision cross sections.

A full exchange calculation was carried out for this $280\,jj$ level approximation for all singlet, triplet, and quintet spin symmetries with total angular momentum $2J \leqslant 14$. This was further augmented with a non-exchange calculation to account for higher partial wave contributions. Due to the long range nature of the Coulomb potential, a further contribution to the dipole allowed transitions come from even higher partial waves.

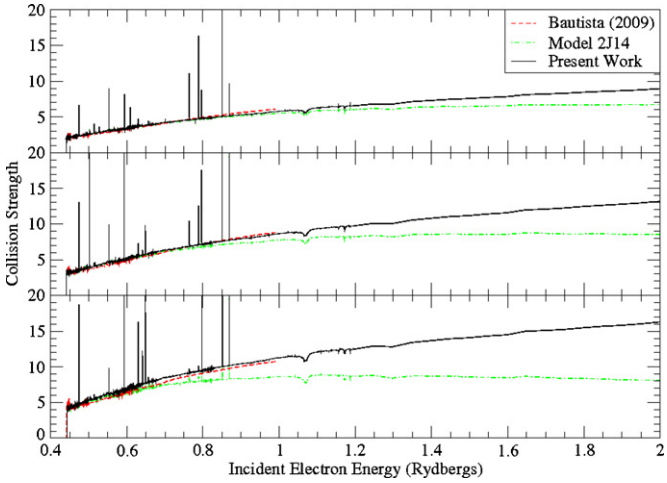

Figure 1. Collision strength against incident electron energy, in Rydbergs, for transitions from the ground state, $3d^5\ ^6S^e_{5/2}$ to the three fine-structure levels of the excited state $3d^44p\ ^6P^o_J$ for $J = 3/2, 5/2$, and $7/2$ (1–83, 1–84, and 1–85), respectively. The solid black line corresponds to the present work, the dot-dashed green line corresponds to Model 2J14, and the dashed red line is the work of Bautista et al. (2009).

(A color version of this figure is available in the online journal.)

We incorporate this "top-up" contribution using the Burgess sum rule for the dipole transitions and a geometric series for the non-dipole transitions, with care being taken to ensure smooth convergence toward the high-energy limit. These important high partial wave contributions were found to be negligible for the low-lying forbidden lines of Cr II considered by Wasson et al. (2010), but as we shall show in the results section are significant for the optically allowed transitions of interest in the present paper.

3. RESULTS AND DISCUSSION

We present in Figures 1–9 the collision strengths, Ω_{ij}, and Maxwellian averaged effective collision strengths, Υ_{ij}, for a selection of dipole allowed transitions in Cr II to investigate convergence and the effects of high partial wave contributions particularly at high incident electron energies. We note that the transitions are labeled according to the index numbers i and j assigned in Table 1. The effective collision strengths are of importance in astrophysical and plasma applications and are obtained by averaging over a Maxwellian distribution of electron

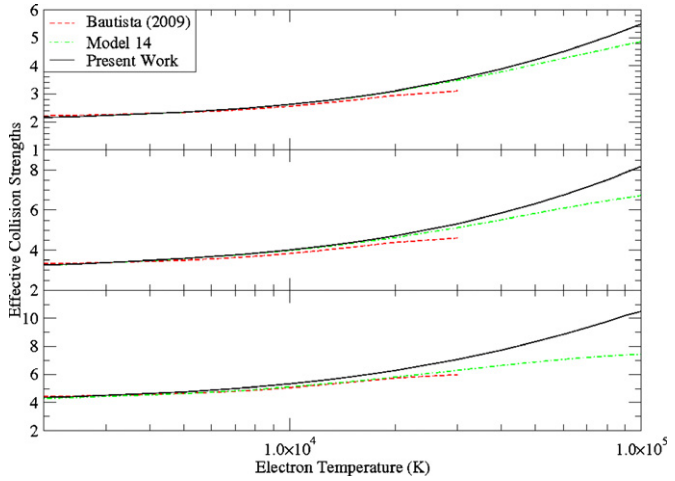

Figure 2. Effective collision strength against electron temperature in Kelvin (log scale), for transitions from the ground state, $3d^5\ ^6S^e_{5/2}$ to the three fine-structure levels of the excited state $3d^4 4p\ ^6P^o_J$ for $J = 3/2, 5/2$, and $7/2$ (1–83, 1–84, and 1–85), respectively. The solid black line corresponds to the present work, the dot-dashed green line corresponds to Model 2J14, and the dashed red line is the work of Bautista et al. (2009).

(A color version of this figure is available in the online journal.)

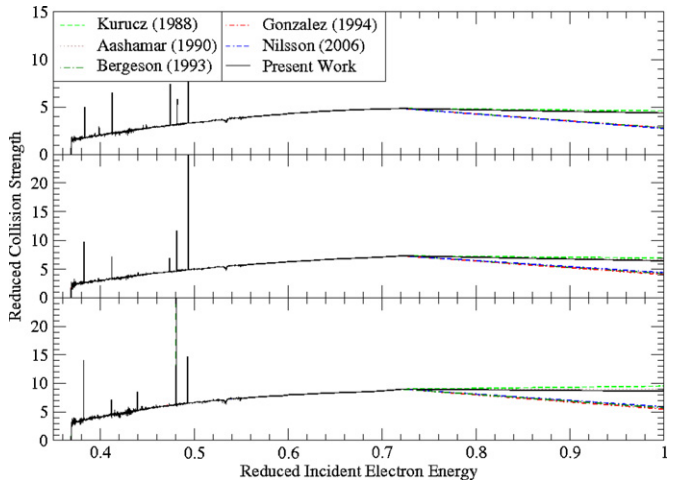

Figure 3. Reduced collision strength against reduced electron temperature, for transitions from the ground state, $3d^5\ ^6S^e_{5/2}$ to the three fine-structure levels of the excited state $3d^4 4p\ ^6P^o_J$ for $J = 3/2, 5/2$, and $7/2$ (1–83, 1–84, and 1–85), respectively.

(A color version of this figure is available in the online journal.)

velocities so that

$$\Upsilon_{ij} = \int_0^\infty \Omega_{ij}(E_j) \exp(-E_j/kT) d(E_j/kT). \qquad (1)$$

Collision strength and effective collision strength comparisons are made with the theoretical work of Bautista et al. (2009) who included all partial waves with angular momentum $L = 0$–10, with higher contributions accounted for via a Coulomb Bethe "top-up" procedure (Burgess 1974). In this work the collision strengths for the fine-structure levels were obtained by algebraic recoupling of the LS reaction matrices (Hummer et al. 1993). The present work includes all partial waves up to and including $2J = 26$ with higher partial wave contributions included via a similar "top-up" procedure. In an attempt to thoroughly investigate the effect of higher partial wave contributions, top-up and convergence of the collision strengths and subsequently the

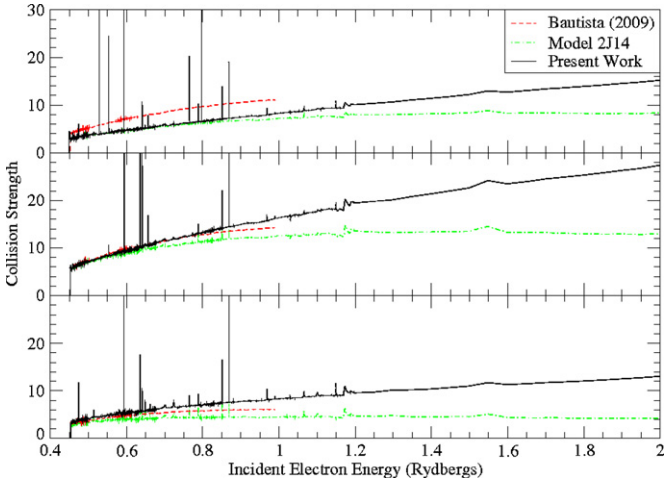

Figure 4. Collision strength against incident electron energy, in Rydbergs, for transitions from the excited state, $3d^4 4s\ ^6D^e_{7/2}$ to the three fine-structure levels of the excited state $3d^4 4p\ ^6D^o_J$ for $J = 5/2, 7/2$, and $9/2$ (5–88, 5–91, and 5–93), respectively. The solid black line corresponds to the present work, the dot-dashed green line corresponds to Model 2J14 and the dashed red line is the work of Bautista et al. (2009).

(A color version of this figure is available in the online journal.)

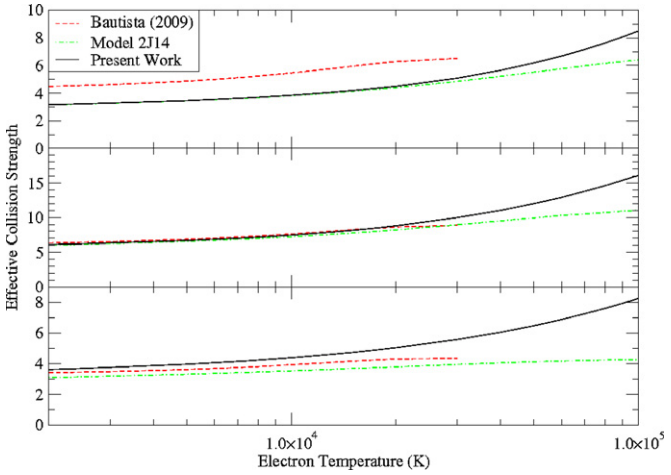

Figure 5. Effective collision strength against electron temperature in Kelvin (log scale), for transitions from the excited state, $3d^4 4s\ ^6D^e_{7/2}$ to the three fine-structure levels of the excited state $3d^4 4p\ ^6D^o_J$ for $J = 5/2, 7/2$, and $9/2$ (5–88, 5–91, and 5–93), respectively. The solid black line corresponds to the present work, the dot-dashed green line corresponds to Model 2J14, and the dashed red line is the work of Bautista et al. (2009).

(A color version of this figure is available in the online journal.)

effective collision strengths, we have also included in our figures the total partial wave contributions up to and including $2J = 14$. This model is referred to as "Model 2J14" and corresponds to the data which would have been produced by the Wasson et al. (2010) investigation for these allowed lines. We remember from this work that convergence of the forbidden lines was the priority and the allowed transitions were not considered. A comparison of data between Model 2J14 and the present work will allow us to thoroughly investigate the contributions from partial waves corresponding to $2J$ values higher than 14.

We consider first transitions from the ground $3d^5\ ^6S^e_{5/2}$ state of Cr II to the odd parity $3d^4 4p\ ^6P^o_J$ state with split levels $J = 3/2, 5/2, 7/2$ (transitions 1–83, 1–84, and 1–85). In Figure 1, we present the collision strength as a function of incident electron energy in Rydbergs for all three dipole allowed

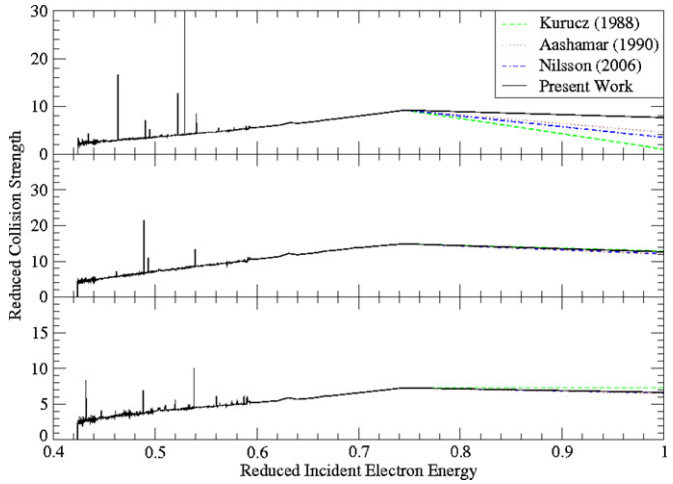

Figure 6. Reduced collision strength against reduced electron temperature, for transitions from the excited state, $3d^4 4s\ ^6D^e_{7/2}$ to the three fine-structure levels of the excited state $3d^4 4p\ ^6D^o_J$ for $J = 5/2, 7/2$, and $9/2$ (5–88, 5–91, and 5–93), respectively.

(A color version of this figure is available in the online journal.)

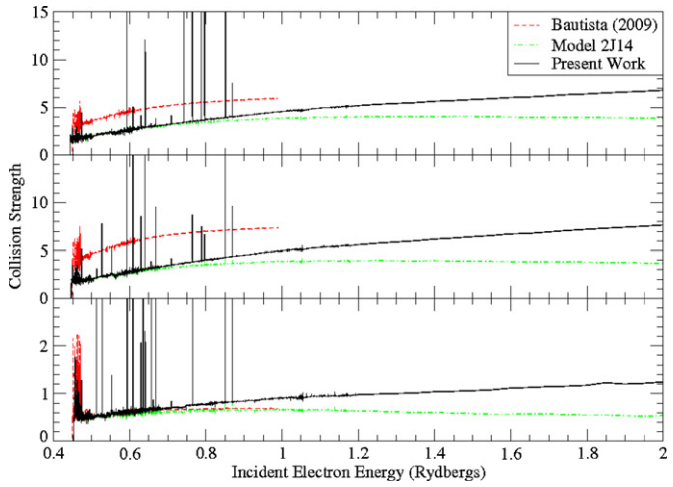

Figure 7. Collision strength against incident electron energy, in Rydbergs, for transitions from the excited state, $3d^4 4s\ ^4D^e_{3/2}$ to the three fine-structure levels of the excited state $3d^4 4p\ ^4P^o_J$ for $J = 1/2, 3/2$, and $5/2$ (8–86, 8–87, and 8–92), respectively. The solid black line corresponds to the present work, the dot-dashed green line corresponds to Model 2J14, and the dashed red line is the work of Bautista et al. (2009).

(A color version of this figure is available in the online journal.)

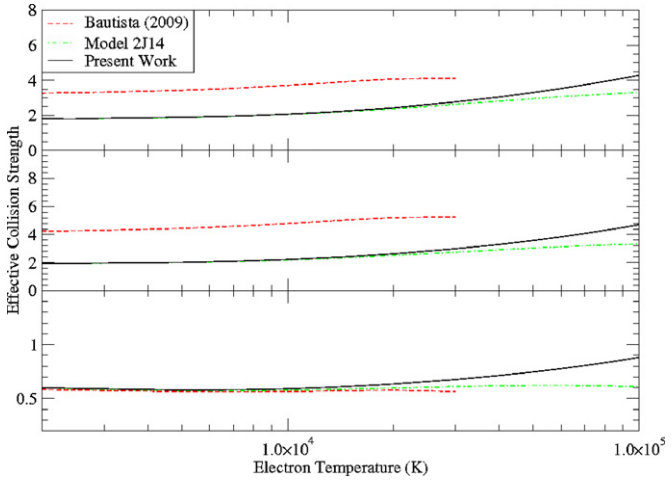

Figure 8. Effective collision strength against electron temperature in Kelvin (log scale), for transitions from the excited state, $3d^4 4s\ ^4D^e_{3/2}$ to the three fine-structure levels of the excited state $3d^4 4p\ ^4P^o_J$ for $J = 1/2, 3/2$, and $5/2$ (8–86, 8–87, and 8–92), respectively. The solid black line corresponds to the present work, the dot-dashed green line corresponds to Model 2J14, and the dashed red line is the work of Bautista et al. (2009).

(A color version of this figure is available in the online journal.)

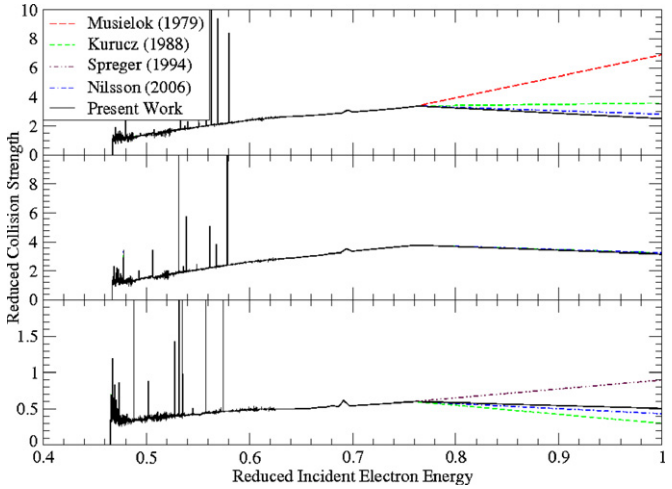

Figure 9. Reduced collision strength against reduced electron temperature, for transitions from the excited state, $3d^4 4s\ ^4D^e_{3/2}$ to the three fine-structure levels of the excited state $3d^4 4p\ ^4P^o_J$ for $J = 1/2, 3/2$, and $5/2$ (8–86, 8–87, and 8–92), respectively.

(A color version of this figure is available in the online journal.)

transitions. The present work and the theoretical cross sections of Bautista et al. (2009) are in excellent agreement up to the highest incident energy of 1 Rydberg. Beyond this energy only the present cross sections are evaluated up to approximately 5 Rydbergs. Differences of only a few percent are recorded for all three transitions between these two works. The collision strengths of Model 2J14 lie, as expected, significantly below the other two, emphasizing the importance of high partial wave contributions and "top-up" for these dipole allowed transitions.

In Figure 2, we present the Maxwellian averaged collision strengths as a function of electron temperature in Kelvin on a logarithmic scale, for the same three transitions. For the lowest temperatures considered ($T = 2000 \rightarrow 10{,}000$ K) excellent agreement is evident between the present results, Bautista et al. (2009) and Model 2J14. Beyond this temperature value deviations occur and at the highest temperature considered the present work indicates effective collision strengths significantly higher than the other predictions. We note the highest temperature considered by Bautista et al. (2009) is T =30,000 K.

As a further check on the accuracy of the atomic data presented in Figures 1 and 2, we can ascertain that our results conform to the expected infinite-energy limits. We utilize the method of Burgess & Tully (1992) where a reduced collision strength, Ω_r is plotted against a reduced energy, E_r, mapping the complete range of incident electron energies onto the interval (0, 1). The reduced energy E_r is calculated as

$$E_r = 1 - \frac{\ln C}{\ln\left(\frac{E_j}{\Delta E} + C\right)}, \qquad (2)$$

where C is an adjustable parameter permitting flexibility, E_j is the incident electron energy following excitation, and ΔE is

Table 2
Oscillator Strengths gf_{ij} Values for Transitions in Cr II Considered in the Figures

i	j	gf_{ij}							
		Present Work	Nilsson et al. (2006)	Spreger et al. (1994)	Gonzalez et al. (1994)	Bergeson & Lawler (1993)	Musielok & Wujec (1979)	Aashamar & Luke (1990)	Kurucz (1988)
1	83	0.48136	0.30061	...	0.30479	0.30903	...	0.48000	0.50466
	84	0.71946	0.48753	...	0.45082	0.46774	...	0.72900	0.76913
	85	0.95880	0.65163	...	0.60814	0.63096	...	0.99100	1.05925
5	88	0.64282	0.28708	...	...	...	...	0.37900	0.08375
	91	1.07536	1.02565	...	...	...	...	1.02100	1.09144
	93	0.56977	0.56105	...	...	...	...	0.52000	0.62373
8	86	0.16673	0.18664	...	...	...	0.45920	...	0.23768
	87	0.21226	0.21677	...	...	...	...	...	0.21677
	92	0.03481	0.02958	0.06166	...	...	...	...	0.02037

Notes. Present work values are taken from the length formula calculations in Table 3. Comparisons are made with the experimental works of Nilsson et al. (2006), Spreger et al. (1994), Gonzalez et al. (1994), Bergeson & Lawler (1993), and Musielok & Wujec (1979) and, finally, the theoretical works of Aashamar & Luke (1990) and Kurucz (1988).

the transition energy between the excited states. The reduced collision strength as a function of the reduced energy is represented by

$$\Omega_r(E_r) = \frac{\Omega(E_j)}{\ln\left(\frac{E_j}{\Delta E} + e\right)}, \quad (3)$$

where e is Euler's constant.

We note that at the infinite-energy limit ($E_r = 1$) the reduced collision strength behaves asymptotically as

$$\Omega_r(E_r) = \frac{4 g_i f_{ij}}{\Delta E}, \quad (4)$$

where g_i is the statistical weight of the initial level ($2J_i + 1$) and f_{ij} denotes the absorption oscillator strength. The infinite-energy limit will clearly vary linearly with the choice of oscillator strength. Table 2 compares the oscillator strengths computed in the present work for the nine transitions considered in this paper with the experimental works of Nilsson et al. (2006), Spreger et al. (1994), Gonzalez et al. (1994), Bergeson & Lawler (1993), and Musielok & Wujec (1979) and, finally, the theoretical works of Aashamar & Luke (1990) and Kurucz (1988).

In Figure 3, we present the reduced collision strength Ω_r as a function of reduced incident electron energy E_r for the three transitions $3d^5\ {}^6S^e_{5/2} \rightarrow 3d^4 4p\ {}^6P^o_{3/2,\,5/2,\,7/2}$ (transitions 1–83, 1–84, and 1–85) considered in Figures 1 and 2. Comparisons are made with the reduced plots formed using the variety of available theoretical and experimental oscillator strengths in Table 2. From Figure 3, we see that the infinite-energy limits predicted by the present work are in very good agreement with the predictions using the f-values of Kurucz (1988) and Aashamar & Luke (1990) but slightly higher than those evaluated using the Nilsson et al. (2006) and Gonzalez et al. (1994) data, for all three transitions.

In Figure 4, we present the collision strength for dipole allowed transitions from the metastable $3d^4 4s\ {}^6D^e_{7/2}$ (index 5) to the $3d^4 4p\ {}^6D^o_J$ for $J = 5/2, 7/2$, and $9/2$ (indices 88, 91, and 93). Again we see the importance of the high partial wave contributions which are absent in Model 2J14. Agreement is not unsatisfactory with the collision strengths of Bautista et al. (2009) for the $3d^4 4s\ {}^6D^e_{7/2} \rightarrow 3d^4 4p\ {}^6D^o_{7/2,9/2}$ transitions, but his predictions for the $3d^4 4s\ {}^6D^e_{7/2} \rightarrow 3d^4 4p\ {}^6D^o_{5/2}$ lie considerably higher than the present work at all incident electron energies. The Maxwellian averaged effective collision strengths presented in Figure 5 for these three transitions corroborate these findings. Agreement is excellent across the temperature range $T = 2000$–$30{,}000$ K for the $3d^4 4s\ {}^6D^e_{7/2} \rightarrow 3d^4 4p\ {}^6D^o_{7/2,\,9/2}$ transitions, but the Bautista et al. (2009) data lie significantly higher than the present work for the $3d^4 4s\ {}^6D^e_{7/2} \rightarrow 3d^4 4p\ {}^6D^o_{5/2}$ transition. It should also be noted that the present work includes a much more extensive temperature range, $T = 2000$–$100{,}000$ K, than the previous evaluation.

The oscillator strengths for these three transitions are listed in Table 2 where we see excellent agreement between the theories of Kurucz (1988), Aashamar & Luke (1990), the present work, and the experimental values of Nilsson et al. (2006) for the $3d^4 4s\ {}^6D^e_{7/2} \rightarrow 3d^4 4p\ {}^6D^o_{7/2,\,9/2}$ transitions. Differences of less than 2% are found between the present theory and the experimental data of Nilsson for these two transitions. For the $3d^4 4s\ {}^6D^e_{7/2} \rightarrow 3d^4 4p\ {}^6D^o_{5/2}$ transition, however, experiment and theory do not agree with discrepancies of 50% or more evident. We clearly see the effect of these differing oscillator strengths in the reduced energy plots of Figure 6 for these transitions. Excellent agreement is found as expected for the lower two transitions whereas the different f-values predict different high-energy limits for the

Table 3
Theoretical Oscillator Strengths, f, and Transition Probabilities, A, between All Allowed Fine-structure Transitions of Cr II

i	j	$J(i)$	$J(j)$	ΔE	$f_{\rm length}$	$f_{\rm velocity}$	$A_{\rm length}$	$A_{\rm velocity}$
1	76	5/2	3/2	0.22120	4.8747^{-08}	5.7941^{-08}	1.1495^{+02}	1.3664^{+02}
1	77	5/2	5/2	0.22223	1.7075^{-07}	2.0714^{-07}	2.7095^{+02}	3.2869^{+02}
1	78	5/2	7/2	0.22365	2.0445^{-07}	2.5068^{-07}	2.4643^{+02}	3.0216^{+02}
1	83	5/2	3/2	0.22762	8.0226^{-02}	7.8855^{-02}	2.0032^{+08}	1.9690^{+08}
1	84	5/2	5/2	0.22870	1.1991^{-01}	1.1862^{-01}	2.0150^{+08}	1.9935^{+08}
1	85	5/2	7/2	0.23021	1.5980^{-01}	1.5934^{-01}	2.0408^{+08}	2.0350^{+08}
1	87	5/2	3/2	0.23884	1.7733^{-04}	1.7102^{-04}	4.8751^{+05}	4.7016^{+05}
1	88	5/2	5/2	0.23720	5.7059^{-05}	3.2965^{-05}	1.0315^{+05}	5.9591^{+04}
1	90	5/2	3/2	0.23509	1.7151^{-04}	1.3945^{-04}	4.5683^{+05}	3.7144^{+05}
1	91	5/2	7/2	0.23903	1.5607^{-05}	3.0811^{-05}	2.1489^{+04}	4.2423^{+04}

(This table is available in its entirety in a machine-readable form in the online journal. A portion is shown here for guidance regarding its form and content.)

Table 4
Maxwellian Averaged Effective Collision Strengths against Temperature (in Kelvin) for Allowed Fine-structure Transitions of Cr II

i	j	Temperature (K) 2,000	2,300	2,500	5,000	7,500	10,000	13,000	15,000	18,000
		20,000	30,000	40,000	50,000	60,000	70,000	80,000	90,000	100,000
		Effective Collision Strength								
1	76	3.46^{-01}	3.30^{-01}	3.21^{-01}	2.51^{-01}	2.21^{-01}	2.06^{-01}	1.96^{-01}	1.92^{-01}	1.89^{-01}
		1.88^{-01}	1.85^{-01}	1.85^{-01}	1.84^{-01}	1.83^{-01}	1.82^{-01}	1.80^{-01}	1.79^{-01}	1.78^{-01}
1	77	7.82^{-01}	7.26^{-01}	6.95^{-01}	4.89^{-01}	4.11^{-01}	3.71^{-01}	3.44^{-01}	3.32^{-01}	3.19^{-01}
		3.13^{-01}	2.97^{-01}	2.89^{-01}	2.84^{-01}	2.80^{-01}	2.77^{-01}	2.74^{-01}	2.71^{-01}	2.68^{-01}
1	78	7.20^{-01}	6.82^{-01}	6.60^{-01}	5.07^{-01}	4.46^{-01}	4.13^{-01}	3.91^{-01}	3.82^{-01}	3.72^{-01}
		3.67^{-01}	3.54^{-01}	3.49^{-01}	3.46^{-01}	3.44^{-01}	3.42^{-01}	3.40^{-01}	3.38^{-01}	3.36^{-01}
1	83	2.16^{+00}	2.18^{+00}	2.19^{+00}	2.35^{+00}	2.49^{+00}	2.63^{+00}	2.78^{+00}	2.88^{+00}	3.02^{+00}
		3.11^{+00}	3.53^{+00}	3.89^{+00}	4.22^{+00}	4.51^{+00}	4.78^{+00}	5.03^{+00}	5.27^{+00}	5.49^{+00}
1	84	3.27^{+00}	3.30^{+00}	3.32^{+00}	3.58^{+00}	3.80^{+00}	4.01^{+00}	4.24^{+00}	4.38^{+00}	4.59^{+00}
		4.72^{+00}	5.32^{+00}	5.85^{+00}	6.32^{+00}	6.75^{+00}	7.15^{+00}	7.51^{+00}	7.86^{+00}	8.18^{+00}
1	85	4.37^{+00}	4.41^{+00}	4.44^{+00}	4.76^{+00}	5.05^{+00}	5.32^{+00}	5.63^{+00}	5.83^{+00}	6.11^{+00}
		6.28^{+00}	7.07^{+00}	7.74^{+00}	8.33^{+00}	8.85^{+00}	9.33^{+00}	9.77^{+00}	1.02^{+01}	1.05^{+01}
1	87	8.41^{-02}	8.75^{-02}	8.93^{-02}	9.78^{-02}	9.96^{-02}	1.01^{-01}	1.02^{-01}	1.02^{-01}	1.03^{-01}
		1.04^{-01}	1.07^{-01}	1.10^{-01}	1.12^{-01}	1.14^{-01}	1.15^{-01}	1.16^{-01}	1.17^{-01}	1.17^{-01}
1	88	1.09^{-01}	1.10^{-01}	1.10^{-01}	1.19^{-01}	1.29^{-01}	1.38^{-01}	1.45^{-01}	1.49^{-01}	1.54^{-01}
		1.56^{-01}	1.64^{-01}	1.69^{-01}	1.73^{-01}	1.75^{-01}	1.77^{-01}	1.78^{-01}	1.78^{-01}	1.79^{-01}
1	90	7.10^{-02}	7.17^{-02}	7.22^{-02}	7.47^{-02}	7.64^{-02}	7.87^{-02}	8.19^{-02}	8.42^{-02}	8.76^{-02}
		8.98^{-02}	9.96^{-02}	1.07^{-01}	1.13^{-01}	1.17^{-01}	1.20^{-01}	1.23^{-01}	1.25^{-01}	1.26^{-01}
1	91	1.13^{-01}	1.13^{-01}	1.13^{-01}	1.18^{-01}	1.25^{-01}	1.32^{-01}	1.39^{-01}	1.44^{-01}	1.49^{-01}
		1.52^{-01}	1.64^{-01}	1.72^{-01}	1.77^{-01}	1.81^{-01}	1.83^{-01}	1.84^{-01}	1.85^{-01}	1.85^{-01}

(This table is available in its entirety in a machine-readable form in the online journal. A portion is shown here for guidance regarding its form and content.)

$3d^4 4s\ ^6D^e_{7/2} \rightarrow 3d^4 4p\ ^6D^o_{5/2}$ transition in the upper plot. Clearly further investigation into the oscillator strengths for these transitions is necessary.

Finally, in Figures 7–9 we present the collision strength as a function of incident electron energy, the corresponding effective collision strength as a function of electron temperature, and the reduced energy plots of Burgess & Tully (1992), respectively, for the $3d^4 4s\ ^4D^e_{3/2} \rightarrow 3d^4 4p\ ^4P^o_{1/2,\,3/2,\,5/2}$ (8–86, 8–87, and 8–92) transitions. Agreement with the collision strengths of Bautista et al. (2009) in Figure 7 is disappointing, with their predictions lying substantially higher than the present collision strengths for two out of the three transitions. The Maxwellian averaged effective collision strengths derived from these collision strengths and displayed in Figure 8 lie about a factor of two higher at all temperatures considered. The agreement for the $3d^4 4s\ ^4D^e_{3/2} \rightarrow 3d^4 4p\ ^4P^o_{5/2}$ transition is, however, excellent across the temperature range. This would suggest that there is considerable mixing between these fine-structure levels. The source of the differences may also stem from the differing representations for the $3d^4 4s$ states in the two calculations. Finally, in Figure 9 we present the reduced energy plots for these transitions and predict the high-energy limits from a variety of f-value sources. We see from Table 2 that the present data are in excellent agreement with the most recent experimental work of Nilsson et al. (2006) for all three transitions of interest. From Figure 9 the present data are as expected in closest agreement with the predictions of Nilsson et al. (2006).

It is clearly evident from Table 2 that there is a paucity of data currently available in the literature for the oscillator strengths for transitions among the fine-structure levels of Cr II. These data will be of significant use to astrophysicists and plasma physicists in their diagnostic applications and for this reason we present in Table 3 a list of oscillator strengths (f) and transition probabilities (A) for all dipole allowed (E1) transitions among the lowest 274 states (removing the final six unobserved states) of Cr II consisting of configurations $3d^5$, $3d^4 4s$, and $3d^4 4p$. The relativistic configuration-interaction CIV3 code of Hibbert (1975) was utilized in the evaluation of this data set and the $J\pi$ selection rules were adopted. It should be noted that the agreement between length and velocity oscillator strengths is really quite good for the majority of the transitions considered, including those which are significantly weak and the oscillator strength is very small. This is a good indicator of the suitability and accuracy of the model used in the present calculation.

Finally, in Table 4 we tabulate the effective collision strengths computed in the present 280 jj approximation for all of the Cr II allowed transitions considered in the present study. This table will compliment the forbidden line tabulation of Wasson et al. (2010). The transitions in Tables 2–4 are labeled according to the index values assigned in Table 1. Temperatures ranging from $T = 2000$–$100{,}000$ K are included in the tabulation.

4. CONCLUSIONS

In this present work, we have computed collision strengths and Maxwellian averaged effective collision strengths for 8669 allowed transitions among the fine-structure levels of Cr II. This approximation contains all levels associated with even configurations $3d^5$ and $3d^4 4s$ and the odd configuration $3d^4 4p$, leading to a substantial 280jj level, 1932 coupled channel scattering problem. The astrophysically significant effective collision strengths have been calculated for an extensive temperature range of 2000–100,000 K, extending the range of data previously available.

Comparison with the work of Bautista et al. (2009) has led to a few discrepancies. Looking at the first optically allowed transitions from the ground state shows promising agreement between the two calculations. Further investigation, however,

highlights a number of instances where the data of Bautista et al. (2009) predict collision strengths higher than the present work. This inevitably has a knock on effect on the effective collision strengths produced. Despite these differences, the strong agreement observed in many instances shows the close correlation between these two works.

The results presented here signify a large increase in the size and sophistication of the model used and represent the largest scattering calculation performed for Cr II. Care and precision has been taken in building the target model, in ensuring convergence of the collision strengths, particularly for higher incident electron energies and as an added check the reduced collision strengths have shown that the infinite-energy limits are in very good agreement with experimental predictions. Comparison with other theoretical models and experimental calculations have in many instances corroborated our results.

Conclusive assessment of the accuracy of the effective collision strengths presented here still remains difficult, especially since we only have the work of Bautista et al. (2009) with which to compare. The definitive testing of these data will come from subsequent application of these results within the disciplines of astrophysics or plasma physics.

All of the data presented in this paper are available from the authors on request including collision strengths, effective collision strengths, and oscillator strengths. Alternatively, the reader is directed to our Web site http://web.am.qub.ac.uk/apa where all the data are freely available for download.

The authors acknowledge the years of work and dedication of V. M. Burke and C. J. Noble of Daresbury Laboratory (UK) in producing the RMATRX II suite of codes used in the internal region calculation. We also extend our gratitude to M. A. Bautista for providing the full set of data for comparison purposes. The work presented in this paper is supported by STFC and I. R. Wasson is supported by a DEL studentship. This work made use of the facilities of HECToR, the UK's national high-performance computing service, which is provided by UoE HPCx Ltd at the University of Edinburgh, Cray Inc. and NAG Ltd.

REFERENCES

Aashamar, K., & Luke, T. M. 1990, J. Phys. B, 23, L733
Ballance, C. P., & Griffin, D. C. 2004, J. Phys. B, 37, 2943
Bautista, M. A., Ballance, C., Gull, T. R., et al. 2009, MNRAS, 393, 1503
Bergemann, M., & Cescutti, G. 2010, A&A, 522, A9
Bergeson, S. D., & Lawler, J. E. 1993, ApJ, 408, 382
Burgess, A. 1974, J. Phys. B: At. Mol. Phys., 7, L364
Burgess, A., & Tully, J. A. 1992, A&A, 254, 436
Burke, P. G., Burke, V. M., & Dunseath, K. M. 1994, J. Phys. B: At. Mol. Opt. Phys., 27, 5341
Clementi, E., & Roetti, C. 1974, At. Data Nucl. Data Tables, 14, 3
Gonzalez, A. M., Ortiz, M., & Campos, J. 1994, Can. J. Phys., 72, 57
Hibbert, A. 1975, Comput. Phys. Commun., 9, 141
Hummer, D. G., Berrington, K. A., Eissner, W., et al. 1993, A&A, 279, 298
Iijima, T., & Nakanishi, H. 2008, A&A, 482, 865
Kurucz, R. L. 1988, in Trans. IAU, XXB, ed. M. McNally (Dordrecht: Kluwer), 168
Luftinger, T., Fröhlich, H.-E., Weiss, W. W., et al. 2010, A&A, 509, A43
Musielok, J., & Wujec, T. 1979, A&AS, 38, 119
Nilsson, H., Ljung, G., Lundberg, H., & Nielsen, K. E. 2006, A&A, 445, 1165
NIST Atomic Spectra Database 2011, http://physics.nist.gov/PhysRefData
Spreger, R., Schelm, B., Kock, M., Neger, T., & Ulbel, M. 1994, J. Quant. Spectrosc. Radiat. Transfer, 51, 779
Sunderland, A. G., Noble, C. J., Burke, V. M., & Burke, P. G. 2002, Comput. Phys. Comm., 145, 311
Wasson, I. R., Ramsbottom, C. A., & Norrington, P. H. 2010, A&A, 524, A35